*PROCEEDINGS OF THE INTERNATIONAL CONFERENCE NANOMATERIALS: APPLICATIONS AND PROPERTIES*
Vol. 4 No 1, 01NTF13(3pp) (2015)

# Analysis of the Influence of Deposition Conditions on the Structure of the Coating Nb-Al-N

V.I. Ivashchenko[1], P.L. Skrynskiy[1], V.N. Rogoz[2,*], A.I. Kupchishin[3], P. Węgierek[4]

[1] *Frantsevich Institute for Problems of Materials Science, National Academy of Sciences of Ukraine, 3, Kryzhanovskogo Str., 03680 Kyiv, Ukraine*
[2] *Sumy State University, 2, Rymsky Korsakov Str., 40007 Sumy, Ukraine*
[3] *Abai Kazakh National Pedagogical University, 13, Dostyk av., 050010 Almaty, Republic of Kazakhstan*
[4] *Lublin University of Technology, 38A, Nadbystrzycka Str., 20-618 Lublin, Poland*

(Received 20 July 2015; published online 29 August 2015)

Nanocomposite Nb-Al-N films prepared by magnetron sputtering have been studied. It has been found that, in the films, there are two stable crystalline structural states, namely, $NbN_z$ and B1-$Nb_{1-x}Al_xN_yO_{1-y}$, and an amorphous like component related to aluminum oxynitride upon reactive magnetron sputtering. The substructure characteristics are sensitive to the current supplied to an Al target and related to the Knoop nanohardness and hardness, which change within in the ranges of 29-33.5 and 46-48 GPa, respectively. Ab initio calculations for the $NbN_z$ and $Nb_2AlN$ phases and NbN / AlN heterostructures have been performed to interpret the obtained results for the first time.

**Keywords:** XRD, Nanohardness, Nb-Al-N.

PACS numbers: 61.05.C –, 61.05.cp, 68.37.Ps, 61.05.j

## 1. INTRODUCTION

Films based on NbN demonstrate a variety of interesting properties, such as high hardness, electrical conductivity, thermal stability, and chemical inertness [1]. The NbN films are used as cathode materials for the field emission under vacuum in microelectronic devices [2]. It was shown that introduction of Al atoms into the crystal lattice leads to the formation of $Nb_{1-x}Al_xN$ solid solutions. The Nb-Al-N films consist of $Nb_{1-x}Al_xN$ solid solutions with the B1 (rarely, BK, which is the δ'-NbN phase) and B4 structures or their mixtures [3-7]. In $Nb_{1-x}Al_xN$ solid solutions, the B1 structure is more preferable at aluminum concentrations $x$ lower than 0.45. In the range from $x = 0.45$ to 0.71, a mixture of B1 and B4 structures is observed, while at $x > 0.71$, the B4 structure (wurtzite type with a hexagonal structure) is formed [6, 7]. On the other hand, nanocomposite NbN / AlN films have not yet been studied up to now. Thus, the aim of this work was to study Nb-Al-N films, because nanocomposite structures of films with higher mechanical properties as compared to those of films consisting of substitutional $Nb_{1-x}Al_xN$ solid solutions can be formed under specific conditions.

## 2. SAMPLE PREPARATION AND EXPERIMENTAL TECHNIQUE

The Nb-Al-N films were deposited on specularly polished Si(100) plates using a magnetron dc sputtering of Nb (99.9 %) and Al (99.999 %) 4 mm thick targets 72 mm in diameter in argon and nitrogen atmospheres with the following deposition parameters: substrate temperature $T_S = 350$ °C, bias voltage of the substrate $U_B = -50$ V, flow rates $F_{Ar} = 40$ cm$^3$/min, = 13 cm$^3$/min, and operating pressure $p = 0.17$ Pa. The currents supplied to the Al target were $I_{Al} = 50$, 100, 150, 200, 250, and 300 mA, which corresponded to the discharge power densities $P_{Al} = 2.9$, 5.7, 8.6, 11.4, 14.3, and 17.1 W/cm$^2$, respectively. The current supplied to the Nb target was $I_{Nb} = 300$ mA ($P_{Nb} = 17.1$ W/cm$^2$). The base pressure in the vacuum chamber was lower than $10^{-4}$ Pa. The distance between the target and the target holder was 8 cm. The dihedral angle between the targets was ~ 45°. The substrates were cleaned by ultrasonic treatment before placing them into the chamber. In addition, the substrates were etched in the vacuum chamber in a hydrogen plasma for 5 min before the deposition. The structural and mechanical properties were analyzed as functions of $P_{Al}$. The coating structure was studied using X-ray diffraction (XRD, Dron 3M diffractometer, $CuK_\alpha$ radiation). When the complex diffraction profiles were superposed, they were separated using the program developed by the authors. The substructure characteristics (crystallite size and microstrain) were determined by an approximation method using the Cauchi function as the approximating function. The Fourier spectra were measured on a TSM 1202 (LTD Infraspek) spectrometer in the range of 400-4000 cm$^{-1}$ at room temperature. The Knoop hardness (HK) was estimated using a Microhardness Tester Micromet 2103 BUEHLER LTD equipped with a Berkovich indenter. Loads were chosen based on the following condition: the indenter penetration should be not higher than 10-20 % of the film thickness. The elastic modulus was measured in a dynamic mode on a Triboindenter TI-950 (HYSITRON) apparatus. The film thickness was determined using a "Micron-gamma" optic profilometer. The thickness of Nb-Al-N coatings $d$ weakly depended on $P_{Al}$. The values of d were in the range of 0.7-0.9 μm.

## 3. RESULTS AND DISSCUSSION

Figure 1a shows the X-ray diffraction patterns of the Nb-Al-N films at different powers $P_{Al}$. The marked peaks correspond to the B1-$NbN_z$ structure [8]. The

* v.rogoz2009@gmail.com

 

patterns demonstrate a halo-like component from an amorphous phase in the diffraction angle range $2\theta = 18\text{-}30°$; the component can be identified as the aluminum nitride amorphous phase based on previous studies. It is seen that reflection (200) is the main reflection. It follows that crystallites with the dominant growth orientation along axis [100] perpendicular to the surface plane are formed at all $P_{Al}$ and a relatively low constant bias potential on the substrate of ~ 50 V. The X-ray diffraction patterns show that reflections (200) and (400) are asymmetric (to the side of larger angles). Separation of these reflection profiles shows the existence of two components with similar types of the crystal lattices but two characteristic lattice parameters. Figure 1b shows the result of the deconvolution of the peaks (200) and (400) into Gaussians for the film deposited at 150 mA (Fig. 1a, curve 3). In Fig. 1b, curves 1 correspond to cubic niobium nitride with lattice parameter $a = 0.439\text{-}0.438$ nm. Gaussian curve 2 can be assigned to a cubic NbN with a low content of substituting aluminum with $a = 0.428\text{-}0.429$ nm, which is characteristic of the Nb-Al-N system with the proportion of aluminum and niobium atoms in the crystal lattice of 1/2 (approximate composition $Nb_{0.67}Al_{0.33}N$). The latter was determined based on the Vegard's law for one type crystal lattices when substituting atoms of different radii [9]. In this case, the base lattice parameters are 0.4393 and 0.4120 nm for B1-$NbN_z$ and B1-AlN, respectively. As $P_{Al}$ increases, the Gaussian peak positions are almost unchanged but the peak intensities increase. At high currents, the proportion of the $NbN_z$ / $Nb_{0.67}Al_{0.33}N$ phases is almost 3/5.

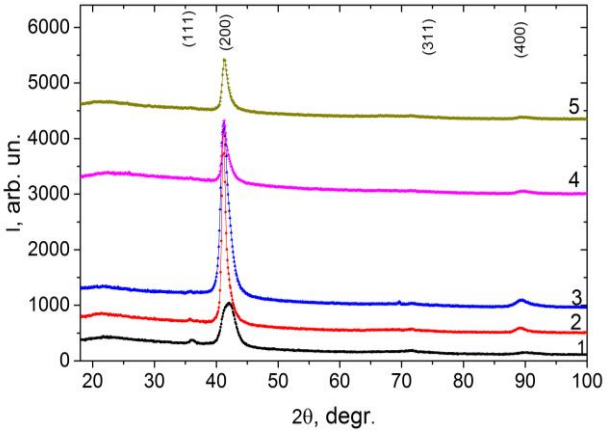


**Fig. 1** – X□ray diffraction patterns of the Nb-Al-N coatings deposited at $P_{Al}$ = 2.9 (1), 5.7 (2), 8.6 (3), 14.3 (4), and 17.1 W/cm² (5)

To determine the substructure characteristics, we used the method of approximation of two orders of the diffraction reflections. We used the (200)-(400) pair. The results of determining the substructure characteristics are shown in Fig. 3. It is seen that the crystallite size and the microstrain increase in the direction of the [100] texture axis for both $NbN_z$ crystallites (dependences 1 in Fig. 3) and crystallites of the $Nb_{0.67}Al_{0.33}N$ phase (dependences 2 in Fig. 3) as power $P_{Al}$ increases. The sharp decrease in the crystallite size and the microstrain at the highest current $P_{Al}$ = 17.1 W/cm² can be due to the annealing and the ordering of the defect structure with the formation of new boundaries by type of the polygonization process. A higher microstrain in $Nb_{0.67}Al_{0.33}N$ crystallites (dependence 2 in Fig. 3b) is likely determined by dissolution of aluminum atoms in the niobium lattice, which strongly distorts the lattice.

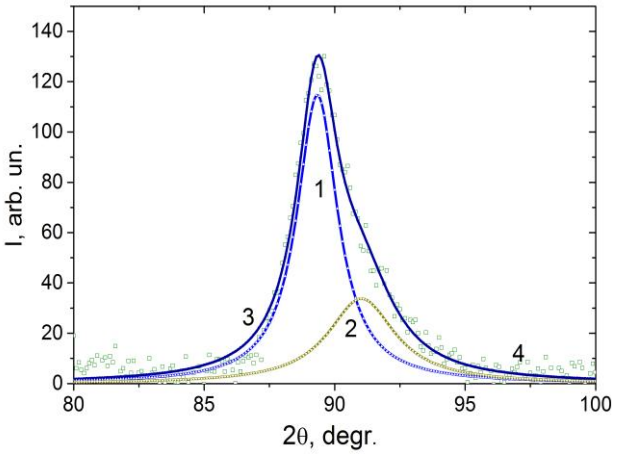


**Fig. 2** – A fragment with separation into components of the diffraction profile of the Nb-Al-N coatings deposited at $P_{Al}$ = 8.6 mA: (1) $NbN_z$, (2) $Nb_{0.67}Al_{0.33}N$, (3) total approximating curve, and (4) points of the initial data array

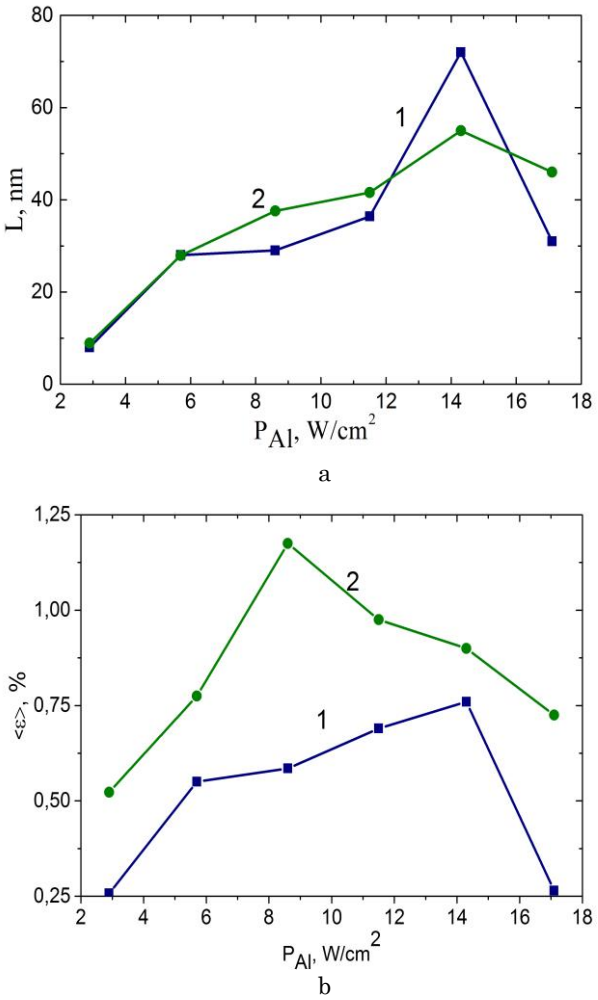


**Fig. 3** – Dependences of the substructure characteristics (a) average crystallite size $L$ and (b) microstrain $\varepsilon$ on $P_{Al}$ for different crystalline components: (1) NbN, (2) $Nb_{0.67}Al_{0.33}N$ (or $Nb_2AlN$)

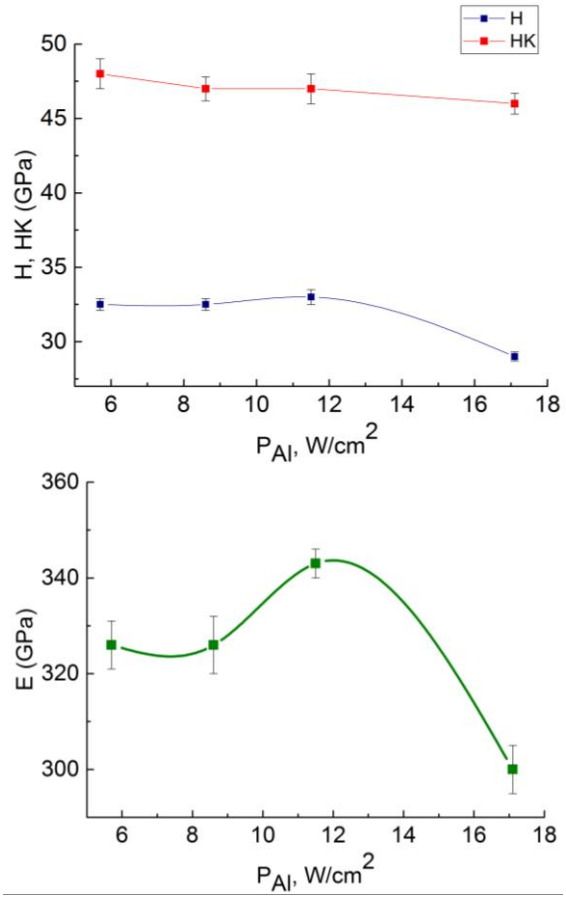


**Fig. 4** - (a) Nanohardness (H), Knoop hardness (HK), and (b) elastic modulus (E) as functions of IAl for the $Nb_{0.67}Al_{0.33}N$ coatings.

We deposited AlN films at different powers $P_{Al}$. The X-ray diffraction patterns show that all the AlN films are amorphous ($\alpha$-AlN, the patterns are not shown in this work). The infrared absorption spectra of the AlN films show that the number of the Al-N bonds increases with $P_{Al}$ (the absorption band at 667 cm$^{-1}$ related to the Al-N vibrations becomes more noticeable). Based on these results, it can be suggested that the films have two stable crystalline structural states: $B1$-NbN and a solid solution with the composition close to $B1$-$Nb_{0.67}Al_{0.33}N$. The films also contain an amorphous-like component related to aluminum nitride. Thus, the films exhibit a nanocomposite structure and consist of $B1$-$NbN_z$ and $B1$-$Nb_{1-x}Al_xN$ nanocrystallites introduced into the $\alpha$-AlN matrix.

The results of nanoindentation and microindentation of the films deposited are shown in Fig. 4. A comparison of the results presented in Figs. 3 and 4 shows that there is a correlation between the mechanical characteristics and the microstrains in the Nb-Al-N films. The nanohardness, the elastic modulus, and the Knoop hardness are maximal in the Nb-Al-N films with grain sizes of 30-40 nm. The increase in the nanohardness from 28 GPa in the NbN film [11] to 32 GPa in the Nb-Al-N films is likely due to the formation of a nanocomposite structure of this film [12-17]. We find that the Knoop hardness is ~ 50 % higher than the nanohardness. This circumstance can be due to that the nanoindentation is performed in a dynamic mode, while the Knoop hardness is determined at static conditions.

## 4. CONCLUSION

Thus, we studied the Nb-Al-N films deposited on silicon substrates by magnetron sputtering of Nb and Al targets at different discharge powers on the Al targets. The experimental studies showed that the films prepared using the chosen deposition parameters have a nanocomposite structure and consist of nanocrystallites B1-$NbN_z$ and B1-$Nb_{1-x}Al_xN_yO_{1-y}$ embedded in the $\alpha$-AlNO matrix. The nanocomposite coating demonstrates high values of hardness (to 32 GPa) as a result of microstrains due to the difference between the atomic radii of the metallic components of the crystal lattices. Taking into account the mechanical properties of the deposited nanocomposite films, these films can be recommended as wear-resistant and protective coatings.

## AKNOWLEDGEMENTS

This study was performed within the framework of the Complex State Programs “Development of the Principles of the Formation of Superhard Nanostructured Coatings with High Physical and Mechanical Properties” (project no. 0112u001382) and “Physical Principles of Plasma Technologies for Complex Processing of Multicomponent Materials and Coatings” (project no. 0113u000137c).

## REFERENCES

1. S.A. Barnett, A. Madan, I. Kom, K. Martin, *MRS Bull.* **169** No3, 169 (2003).
2. Y. Gotoh, M. Nagao, T. Ura, H. Tsuji, J. Ishikawa, *Nucl. Instr. Meth. Phys. Res. B* **148** No1-4, 925 (1999).
3. T.I. Selinder, D.J. Miller, K.E. Gray, *Vacuum* **46** No12, 1401 (1995).
4. Y. Makino, K. Saito, Y. Murakami, K. Asami, *Solid State Phenom*. **127**, 195 (2007).
5. H.C. Barshilla, B. Deepthi, K.S. Rajam, *J. Mater. Res.* **23** No5, 1258 (2008).
6. R. Franz, M. Lechthaler, C. Polzer, C. Mitterer, *Surf. Coat. Technol.* **204** No15, 2447 (2010).
7. D. Holec, R. Franz, P.H. Mayrhofer, C. Mitterer, *J. Phys. D* **41**, 145403 (2010).
8. 038-1155 – *XRD data files*.
9. Я.С. Уманский, Ю.А. Скаков, *Физика металлов. Атомное строение металлов и сплавов* (М.: Атомиздат.: 1978).
10. K. Jadannadham, A.K. Sharma, Q. Wei, R. Kalyanraman, J. Narayan, *J. Vac. Sci. Technol. A* **16**, 2804 (1998).
11. V.I. Ivashchenko, S. Veprek, P.L. Scrynskyy, O. Lytvyn, O.O. Butenko, O.K. Sinelnichenko, L. Gorb, F. Hill, J. Leszczynski, and A.O. Kozak *J. Superhard Mater*. **36** No6, 1 (2014).
12. A.D. Pogrebnjak, E.A. Bazyl, *Vacuum* **64** No1, 1 (2001).
13. A.D. Pogrebnjak, S.M. Ruzimov, *Phys. Lett. A* **120** No5, 259 (1987).
14. V.I. Lavrentiev, A.D. Pogrebnjak, *Surf. Coat. Technol.* **99** No1-2, 24 (1998).
15. P. Misaelides, A. Hatzidimitriou, F. Noli, A.D. Pogrebnjak, Y.N. Tyurin, S. Kosionidis, *Surf. Coat. Technol.* **180-181**, 290 (2004).
16. A.D. Pogrebnyak, D.I. Proskurovskii, *phys. status solidi a* **145** No 1, 9 (1994).
17. A.D. Pogrebnjak, O.G. Bakharev, N.A. Pogrebnjak, Yu.V. Tsvintarnaya, V.T. Shablja, R. Sandrik, A. Zecca, *Phys. Lett. A* **265** No3, 225 (2000).